IEEE Photonics Journal
An IEEE Photonics Society Publication

Open Access

A Variational Method to Solve Waveguide Problems by Employing Dynamic Programming Technique

Volume 6, Number 5, October 2014

Yan Ju Chiang
Likarn Wang

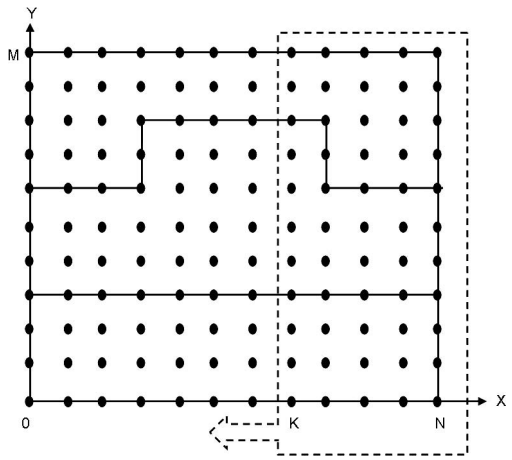

DOI: 10.1109/JPHOT.2014.2353627
1943-0655 © 2014 IEEE

IEEE photonics SOCIETY

IEEE

A Variational Method to Solve Waveguide Problems by Employing Dynamic Programming Technique

Yan Ju Chiang[1] **and Likarn Wang**[2]

[1]Department of Electronics Engineering, Oriental Institute of Technology, Taipei 22061, Taiwan
[2]Institute of Photonics Technologies, College of Electrical Engineering and Computer Science, National Tsing Hua University, Hsinchu 30013, Taiwan

DOI: 10.1109/JPHOT.2014.2353627

Manuscript received July 26, 2014; revised August 23, 2014; accepted August 27, 2014. Date of publication September 5, 2014; date of current version September 11, 2014. This work was supported in part by the National Science Council under Grant NSC 101-2221-E-161-007 and Grant 102-2221-E-007-089 and by the National Tsing Hua University under Grant 102N2080E1. Corresponding author: Y. J. Chiang (e-mail: ff039@mail.oit.edu.tw).

Abstract: A new variational method for the modal analysis of 2-D waveguide structures is proposed in this paper. Maxwell's equations describing the modal properties of scalar and semivectorial guided waves in the 2-D waveguides are expressed as variational/minimization problems, which are then discretized in terms of a finite-difference scheme on a finite rectangular computational window. By applying a dynamic programming technique to solve such variational problems, a 1-D equation representing the relation between the modal fields on any pair of adjacent columns in the computational window can be derived. By using such 1-D equation in a stepwise fashion from one boundary column toward the other boundary column, a system of linear equations with the unknown column modal fields can be derived and then solved to give both the accurate modal indexes and the discrete modal fields. In the examples of one weakly guiding rib-type dielectric waveguide and another strongly guiding silicon-on-insulator waveguide, computational results show that a small size of the coefficient matrix for such a system of linear equations is adequate to cause a relative error of 10^{-5}–10^{-6} in the evaluation of the modal indexes reachable in an efficient manner. The results of the convergence tests show that the proposed method is at least an order of magnitude faster than the conventional finite-difference beam propagation method because of the transformation of a 2-D problem into a 1-D problem. Moreover, the proposed method is applied to investigate the modal properties of the conductor-gap-silicon plasmonic waveguide. The feature of the hybrid guided-mode profile is also observable from the modal field calculated by the proposed method.

Index Terms: Waveguides, variational methods, dynamic programming.

1. Introduction

The calculation of the modes is very important in the analysis of the properties of the optical waveguides. In the case of two-dimensional waveguides, considerable efforts have been made in the development of various variational methods for the determination of the modal properties of the optical waveguide over the past two decades. These methods involve the evaluation of the extremum of the Rayleigh's quotient [1]–[10]. However, the methods reported to date show that computationally intensive efforts are still required for precisely evaluating the extremum of

the Rayleigh's quotient because the model of the Rayleigh's quotient is conventionally established by applying the finite-difference [1] or the finite-element techniques [2], [3], and the computational efforts for solving the resulting eigen-value problem will be intensive due to the diagonalization of the large-scale matrices.

To date, many approximation techniques have been developed to evaluate the extremum of the Rayleigh's quotient. A first-order approximation technique has been introduced based on the conventional perturbation theory [4]–[9]. The trial fields are utilized to evaluate the value of the Rayleigh's quotient, which corresponds to the modal index of the waveguide. However, the accuracy of the resulting modal indices would substantially depend on the similarities between the trial fields and the true modal fields. To prevent the numerical inaccuracy occurred in the calculation of modal indices due to the poor choice of the trial fields, a steepest-descent algorithm [10] has been proposed by introducing the parameterized trial fields into Rayleigh's quotient. By optimizing the parameterized Rayleigh's quotient, an improved trial field which may be used to evaluate the modal indices more accurately can be derived. An alternative way to iteratively improve the accuracy of the trial field has been reported by Sharma *et al.* [11]–[14], which assumes that the trial field in the waveguide with a rectangular cross section is separable in x- and y- directions. This separable field defines two equivalent slab waveguide structures. Then by iteratively evaluating the index distribution and the modal properties of each slab waveguide, the accuracy of the trial field can be effectively improved. Recently, a variational method combined with an efficient effective index method has been reported [15]. However, effective index method only can accurately evaluate the modal properties of the weakly-guiding waveguides [16].

An alternative approach to accurately solve the variational waveguide problem and simultaneously avoid the diagonalization of the large-scale matrices might be the dynamic programming technique, which has been used in various fields since the original work first published by Bellman in 1957 [17]. Conceptually speaking, the dynamic programming is a kind of divide-and-conquer technique, which can be used to solve a large-scale optimization problem in a recursive manner [18]. In the next Section, we will show that the dynamic programming technique can be employed to solve the large-scale, waveguide problem in such a way that by applying an alternative functional formulation, which has been used over decades [19]–[22] rather than the Rayleigh's quotient, the original waveguide problem can be transformed into a series of the variational sub-problems defined in recursively partitioning domains within the cross section of the waveguide. Meanwhile, the dynamic programming technique can be applied to recursively solve these variational sub-problems. As a result, a 1-D relation illustrating the modal fields on any pair of adjacent columns in the computational window can be derived. The method proposed in this paper utilizes the one-dimensional relation to investigate the modal properties of the optical waveguide.

The paper is organized as follows. The theory of the proposed method is outlined for the case of scalar and semivectorial, quasi-TM modes in Sections 2 and 3, respectively. We will show in Section 3 that due to the lack of the functional expression for which the Euler–Lagrange equation [23] is the quasi-TM wave equation for the modal fields of the two-dimensional waveguide in an arbitrary geometry, the method proposed in this paper divides the cross section of the waveguide into several slab waveguide regions. We show that there exists the functional expression whose the stationary solution is the part of the modal field in each slab waveguide region. Meanwhile, the stationary solution in each slab waveguide region can be combined to construct the accurate modal field defined in the entire cross section of the waveguide via the consideration of the field continuities at the interfaces between the slab waveguide regions. In Section 4 the proposed methods are compared with the well-known effective index algorithm [16], finite-difference algorithm, and the finite-element algorithm by evaluating their algorithmic performance. In Section 5, the proposed algorithms are applied to investigate the modal properties of a rib-type, weakly guiding dielectric waveguide [24], a strongly guiding, silicon-on-insulator dielectric waveguide [25], and a conductor-gap-silicon plasmonic waveguide [26]. The numerical results are compared with those presented in [24]–[26], as well as the results derived by applying R-Soft BeamPROP. Finally, Section 6 concludes this paper.

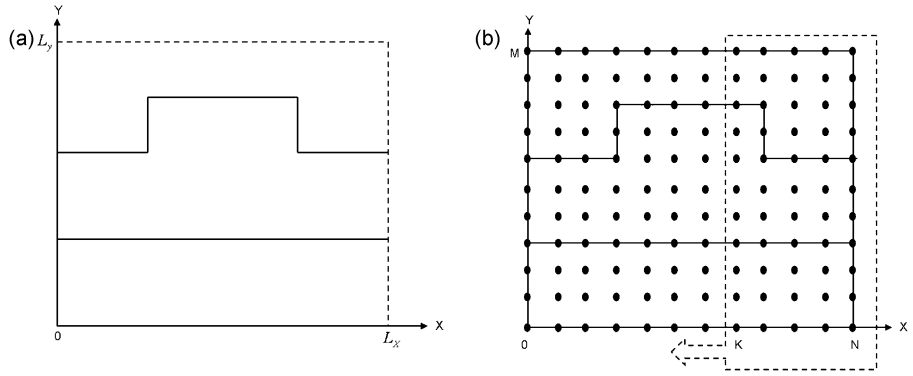

Fig. 1. (a) The computational window $\Omega = L_x \times L_y$ used in the scalar mode calculation. It is enclosed by x–y coordinate axes and the dashed lines. In (b), the solid circles define a $(M+1)\times(N+1)$ mesh used in the scalar mode calculation. As indicated in (7), the function $f_K(v,\beta)$ is the extrema of the functional $J(E_{i,j},\beta)$ in the mesh enclosed by the dashed box. The dashed arrow on the box shows the direction along which the function $f_K(v,\beta)$ can be recursively derived via the recurrence relation (8).

2. Scalar Mode

2.1. Problem Formulation

Fig. 1(a) defines a rib-type waveguide with a permittivity distribution $\varepsilon(x,y)$ in the computational window $\Omega = L_x \times L_y$. The scalar modal field $E(x,y)$ associated with the waveguide is governed by the wave equation [22]

$$\frac{\partial^2 E(x,y)}{\partial x^2} + \frac{\partial^2 E(x,y)}{\partial y^2} + \left(k_0^2 \varepsilon(x,y) - \beta^2\right) E(x,y) = 0 \tag{1}$$

where $k_0 = 2\pi/\lambda$ is the vacuum wave number, and β is the propagation constant. We assume the modal field $E(x,y)$ propagates along the z-direction. The functional $J(E(x,y),\beta)$ [22], in which the modal field $E(x,y)$ is a stationary solution is given by

$$J(E(x,y),\beta) = \iint_{\Omega} \left\{ \left(\frac{\partial E(x,y)}{\partial x}\right)^2 + \left(\frac{\partial E(x,y)}{\partial y}\right)^2 - \left(k_0^2 \varepsilon(x,y) - \beta^2\right) E^2(x,y) \right\} dx\, dy \tag{2}$$

$$E(x, y=0) = E(x, y=L_y) = E(x=L_x, y) = 0 \tag{3}$$

$$E(x=0, y) = 0. \tag{4}$$

Equations (2)–(4) formulate a waveguide problem for scalar modes. The objective is to find the extremum of the functional equation $J(E(x,y),\beta)$ subject to four boundary conditions (3) and (4) at the edges of the computational window Ω.

In Fig. 1(b), we define a $(M+1)\times(N+1)$ mesh as a discrete window in which $E_{i,j} = E(j\Delta, i\Delta)$ and $\varepsilon_{i,j} = \varepsilon(j\Delta, i\Delta)$, $i = 0,1,2,\ldots M$ and $j = 0,1,2,\ldots N$ denote the discrete modal field and the permittivity distribution, respectively. The boundary conditions at the edges of the mesh can be written as $E_{0,j} = E_{M,j} = E_{i,N} = 0$ and $E_{i,0} = 0$ corresponding to the boundary conditions (3) and (4). By using these boundary conditions, the variation functional $J(E_{i,j},\beta)$ corresponding to the functional (2) can be written in terms of $E_{i,j}$ and $\varepsilon_{i,j}$ as

$$\begin{aligned} J(E_{i,j},\beta) &= \sum_{j=1}^{N} \left\{ \sum_{i=1}^{M-1} \left(E_{i,j} - E_{i,j-1}\right)^2 + \sum_{i=2}^{M-1} \left(E_{i,j} - E_{i-1,j}\right)^2 + E_{1,j}^2 + E_{M-1,j}^2 + \sum_{i=1}^{M-1} g_{i,j}(\beta) E_{i,j}^2 \right\} \\ &= \sum_{j=1}^{N} \left\{ u_j^T \left(Q + G_j(\beta)\right) u_j + (u_j - u_{j-1})^T (u_j - u_{j-1}) \right\}. \end{aligned} \tag{5}$$

In the first equality of (5), the function $g_{i,j}(\beta)$ denotes the term $-(k_0^2\varepsilon_{i,j}-\beta^2)\Delta^2$. The second equality shows the functional $J(E_{i,j},\beta)$ in a matrix form via the definitions of the $(M-1)\times 1$ modal field u_j, and the $(M-1)\times(M-1)$ matrices Q and $G_j(\beta)$:

$$u_j=\begin{pmatrix} E_{1,j} \\ E_{2,j} \\ \vdots \\ E_{M-1,j}\end{pmatrix},\quad Q=[Q_{i,j}]=\begin{cases} 2 & i=j=1,2,\ldots,(M-1) \\ -1 & |i-j|=1 \quad i,j=1,2,\ldots(M-1) \\ 0 & \text{otherwise}\end{cases}, G_j(\beta)=\text{diag}\begin{pmatrix} g_{1,j}(\beta) \\ g_{2,j}(\beta) \\ \vdots \\ g_{M-1,j}(\beta)\end{pmatrix}. \tag{6}$$

Note that it is easy to verify that the matrix Q is positive definite and thus the coefficient matrix $Q+G_j(\beta)+I$ in the quadratic term $u_j^T(\cdot)u_j$ in (5) can be made to be positive definite by appropriately choosing the mesh grid size Δ. The positive definiteness embedded in the coefficient matrix $Q+G_j(\beta)+I$ implies that given a fixed value of β there exists the minimum of the functional $J(E_{i,j},\beta)$ with respect to the modal field u_j.

2.2. Dynamic Programming Technique

To calculate the modal field u_j which minimizes the functional $J(E_{i,j},\beta)$, for each positive K we define a solution $f_K(v,\beta)$ of the sub-problem associated with the problem (5) as

$$\begin{aligned} f_K(v,\beta) &= \min_{u_K,u_{K+1},\ldots u_N}\sum_{j=K}^{N}\left\{u_j^T\left(Q+G_j(\beta)\right)u_j+(u_j-u_{j-1})^T(u_j-u_{j-1})\right\} \\ &= \min_{u_K}\Bigg\{u_K^T(Q+G_K(\beta))u_K+(u_K-v)^T(u_K-v) \\ &\qquad +\min_{u_{K+1},u_{K+2},\ldots u_N}\sum_{j=K+1}^{N}\left[u_j^T\left(Q+G_j(\beta)\right)u_j+\left(u_j-u_{j-1}\right)^T(u_j-u_{j-1})\right]\Bigg\} \end{aligned} \tag{7}$$

where $v=u_{K-1}$. Given a fixed value of β the function $f_K(v,\beta)$ is the extrema of the functional $J(E_{i,j},\beta)$ in the mesh $[0\ M\Delta]\times[K\Delta\ N\Delta]$, as shown in Fig. 1(b). The last equality in (7) shows that the function $f_K(v,\beta)$ can be written in a recursive form

$$\begin{aligned} f_K(v,\beta) &= \min_{u_K}\left\{u_K^T(Q+G_K(\beta))u_K+(u_K-v)^T(u_K-v)+f_{K+1}(u_K,\beta)\right\} \\ &\qquad v=u_{K-1},K=1,2,\ldots(N-1) \\ f_N(u_{N-1}) &= u_N^T(Q+G_N(\beta))u_N+(u_N-u_{N-1})^T(u_N-u_{N-1})=u_{N-1}^Tu_{N-1}=|u_{N-1}|^2. \end{aligned} \tag{8}$$

Equation (8) shows that the function $f_K(v,\beta)$ can be solved recursively from $K=N$ to $K=1$ and the terminal function $f_1(v,\beta)=\min_{u_1,u_2,\ldots u_N}\{J(E_{i,j},\beta)\}$ solves the original waveguide problem (5). Note the pure quadratic form in the function $f_N(u_{N-1})$ holds due to Dirichlet's boundary condition at the edge of the mesh, i.e., $u_N=(E_{i,N})=0$, $i=1,2,\ldots(M-1)$. It is intuitive to assume that for each positive K the function $f_K(v,\beta)$ has also a pure quadratic form: $f_K(v,\beta)=v^TC_K(\beta)v$. By substituting the function $f_{K+1}(u_K,\beta)=u_K^TC_{K+1}(\beta)u_K$ into the recurrence relation (8), and algebraically carrying out the quadratic minimization over u_K, both iterative relations for the modal field u_K and the coefficient matrix $C_K(\beta)$ can be derived as

$$\begin{aligned} C_K(\beta) &= I-(I+Q+G_K(\beta)+C_{K+1}(\beta))^{-1},\quad K=1,2,\ldots(N-1) \\ u_K &= (I-C_K(\beta))u_{K-1} \end{aligned} \tag{9}$$

where $C_N(\beta)=I$ followed by the observation on the function $f_N(u_{N-1})=u_{N-1}^2$. Based on the Dirichlet's boundary condition (4) at $x=0$, i.e., $u_0=(E_{i,0})=0$, the iterative relation for modal

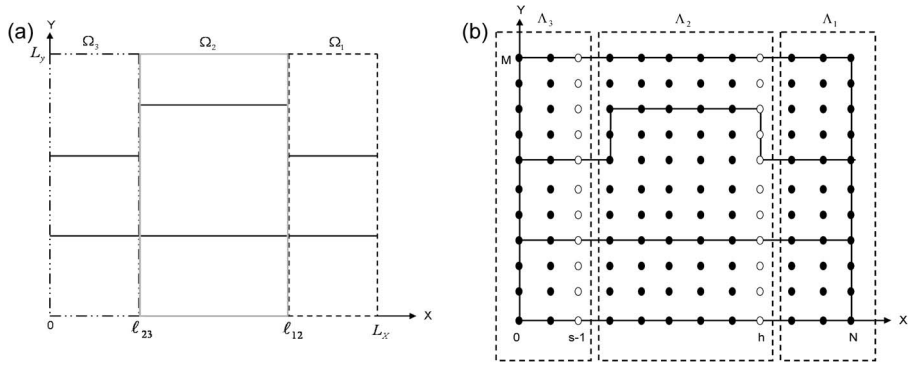

Fig. 2. (a) The computational window $\Omega = \Omega_1 \cup \Omega_2 \cup \Omega_3 = L_x \times L_y$ used in the quasi-TM mode calculation is divided into three slab waveguide regions. The regions enclosed by dashed lines, gray lines, and dashed-dot lines define the divided slab waveguides Ω_1, Ω_2, and Ω_3, respectively. $x = \ell_{12}$ and $x = \ell_{23}$ denote the interfaces between the slab waveguide regions. In (b), the circles define a $(M+1) \times (N+1)$ mesh $\Lambda = \Lambda_1 \cup \Lambda_2 \cup \Lambda_3$ used in the quasi-TM mode calculation. The mesh is divided into three slab waveguide regions in such a way that the mesh points enclosed by the dashed boxes from the right to the left sides in the figure construct the slab waveguides Λ_1, Λ_2, and Λ_3. The two sets of empty circles $L_{12} = \{(i\Delta, j\Delta) | 0 \le i \le M\ j = h)\}$ and $L_{23} = \{(i\Delta, j\Delta) | 0 \le i \le M\ j = s-1)\}$ define the interfaces between the slab waveguide regions.

field u_0 and u_1 can be written as $(I - C_1(\beta))^{-1} u_1 = u_0 = 0$. This equation and (9) form a new algorithm which is capable to calculate the propagation constant β and the corresponding discrete modal field u_K for $K = 0, 1, 2, \ldots, (N-1)$. First the equation (9) is applied to evaluate the coefficient matrix $C_K(\beta)$ sequentially until the last coefficient matrix, $C_1(\beta)$, is derived. Then the propagation constant β can be derived via solving the equation $\det[(I - C_1(\beta))^{-1}] = 0$.

Although the equation $\det[(I - C_1(\beta))^{-1}] = 0$ is a nonlinear equation and must be solved via well-known algorithms such as Newton's like solver, the numerical results in Section 4 will demonstrate that by appropriately selecting the initial value of β, the accurate value of β can be derived in an efficient manner. Once the final value of β has been determined, the modal field u_1 can be calculated via solving a system of $(M-1)$ linear equations $(I - C_1(\beta))^{-1} u_1 = 0$. Finally, the other modal fields u_K for $K = 2, \ldots, (N-1)$ can be derived by employing (9).

3. Quasi-TM Mode

3.1. Problem Formulation

In this section we adopt the same notations as those used in scalar-mode theory. Fig. 2(a) defines a rib-type waveguide with a permittivity distribution $\varepsilon(x, y)$ in the computational window $\Omega = \Omega_1 \cup \Omega_2 \cup \Omega_3 = L_x \times L_y$, in which the y-polarized modal field $E_y(x, y)$ is governed by the wave equation for quasi-TM modes [22]

$$\frac{\partial^2 E_y(x,y)}{\partial x^2} + \frac{\partial^2 E_y(x,y)}{\partial y^2} + \frac{\partial}{\partial y}\left(\frac{1}{\varepsilon(x,y)} \frac{\partial \varepsilon(x,y)}{\partial y} E_y(x,y)\right) + \left(k_0^2 \varepsilon(x,y) - \beta^2\right) E_y(x,y) = 0 \qquad (10)$$

where $k_0 = 2\pi/\lambda$ and β denote the vacuum wave number and the corresponding propagation constant, respectively. To derive the variation functional with respect to the wave equation (10) for the rib-waveguide in Fig. 2(a), the corresponding permittivity distribution $\varepsilon(x, y)$ is divided into three disjoint slab waveguides, i.e., $\varepsilon(x, y) = \sum_{m=1}^{3} \varepsilon(x, y) \cdot U_m(x, y)$, where the unit-step function $U_m(x, y)$ is defined in such a way that $U_m(x, y) = 1$, $(x, y) \in \Omega_m$, otherwise $U_m(x, y) = 0$. For notational simplicity, because the term $\varepsilon(x, y) \cdot U_m(x, y)$ is zero outside the slab waveguide region Ω_m, in the following contents of this section we use functions $\varepsilon_m(y \in \Omega_m)$, $m = 1, 2, 3$ to define the permittivity distribution in the local slab waveguide region Ω_m, i.e., $\varepsilon_m(y \in \Omega_m) = \{\varepsilon(x, y) \cdot U_m(x, y) | (x, y) \in \Omega_m\}$. Note that in each slab waveguide region

Ω_m, the permittivity is invariant along the x direction, as shown in Fig. 2(a); so, the function $\varepsilon_m(\cdot)$ depends only on the variable y.

In Fig. 2(a), we introduce $x = \ell_{12}$ and $x = \ell_{23}$ as the interfaces between the slab waveguide regions. Again we partition the modal field $E_y(x, y)$ into three parts, i.e., $E_y(x, y) = \sum_{m=1}^{3} E_y(x, y) \cdot U_m(x, y)$, where the partial field $E_y(x, y) \cdot U_m(x, y)$ is zero outside the local slab waveguide region Ω_m,. In the following contents of this section, for notational simplicity, we define a function $E_y^m((x, y) \in \Omega_m) = \{E_y(x, y) \cdot U_m(x, y) | (x, y) \in \Omega_m\}$ to represent the part of the modal field $E_y(x, y)$ in the local slab waveguide region Ω_m.

While the above partitions of the modal field $E_y(x, y)$ and the permittivity distribution $\varepsilon(x, y)$ are substituted into the wave (10), it can be seen that every local field $E_y^m((x, y) \in \Omega_m)$ is governed by the (10) defined in each local slab waveguide region Ω_m. Furthermore, there exists the functional $\min_{E_y^m} \iint_{\Omega_m} F_m(E_y^m(x, y), \varepsilon_m(y), \beta)\, dx\, dy$ for which Euler–Lagrange equation [23] is the quasi-TM wave (10) defined in each local slab waveguide region Ω_m. The stationary solution of the functional corresponds to the local field $E_y^m((x, y) \in \Omega_m)$. By summing up all functionals defined in the local slab waveguide regions, we may define the variational problem $J_{\text{rib-TM}}(E_y(x, y), \beta)$ in the computational window $\Omega = \Omega_1 \cup \Omega_2 \cup \Omega_3$ as

$$\begin{aligned} J_{\text{rib-TM}}\big(E_y(x, y), \beta\big) &= \sum_{m=1,2,3} \min_{E_y^m} \iint_{\Omega_m} F_m\Big(E_y^m(x, y), \varepsilon_m(y), \beta\Big)\, dx\, dy \\ &= \sum_{m=1,2,3} \min_{E_y^m} \iint_{\Omega_m} \varepsilon_m(y) \Bigg\{ \left(\frac{\partial E_y^m}{\partial x}\right)^2 + \left(\frac{\partial E_y^m}{\partial y}\right)^2 \\ &\qquad - \left[\frac{\partial}{\partial y}\left(\frac{1}{\varepsilon_m(y)} \cdot \frac{\partial \varepsilon_m(y)}{\partial y}\right) + k_0^2 \varepsilon_m(y) - \beta^2\right] \left(E_y^m\right)^2 \Bigg\}\, dx\, dy \end{aligned} \tag{11}$$

$$E_y^m(x, y = 0) = E_y^m x, y = L_y) = 0, \quad E_y^1(x = L_x, y) = 0, \quad m = 1, 2, 3 \tag{12}$$

$$E_y^3(x = 0, y) = 0 \tag{13}$$

$$E_y^1(x = \ell_{12}, y) = E_y^2(x = \ell_{12}, y), \quad E_y^2(x = \ell_{23}, y) = E_y^3(x = \ell_{23}, y) \tag{14}$$

$$-j\omega\mu \cdot H_x^1(x = \ell_{12}, y) = \frac{\partial E_y^1(x = \ell_{12}, y)}{\partial x} = \frac{\partial E_y^2(x = \ell_{12}, y)}{\partial x} = -j\varpi\mu \cdot H_z^2(x = \ell_{12}, y) \tag{15}$$

$$-j\varpi\mu \cdot H_x^2(x = \ell_{23}, y) = \frac{\partial E_y^2(x = \ell_{23}, y)}{\partial x} = \frac{\partial E_y^3(x = \ell_{23}, y)}{\partial x} = -j\varpi\mu \cdot H_z^3(x = \ell_{23}, y) \tag{16}$$

where $H_z^m(x, y)$ denotes the z-polarized magnetic field corresponding to the field $E_y^m(x, y)$ and μ is the permeability of the material in the window Ω. Equations (12) and (13) are Dirichlet's boundary conditions imposed on four edges of the window Ω. In equations (14)–(16), we introduce the field $E_y^m(x, y)$ and $H_z^m(x, y)$ continuities at interfaces $x = \ell_{12}$ and at $x = \ell_{23}$, respectively.

Based on the linearity of the functional expression $J_{\text{rib-TM}}(E_y(x, y), \beta)$ shown in (11) and the principle of the optimality, the variational waveguide problem $J_{\text{rib-TM}}(E_y(x, y), \beta)$ can be separately solved via the minimization of the functional (11) in each slab waveguide region Ω_m, i.e., the minimization of the functional $\iint_{\Omega_m} F_m(E_y^m(x, y), \varepsilon_m(y), \beta)\, dx\, dy$. To derive the discrete variational model with respect to the functional (11) in each slab waveguide region Ω_m, Fig. 2(b) shows a $(M + 1) \times (N + 1)$ mesh $\Lambda = \Lambda_1 \cup \Lambda_2 \cup \Lambda_3$ in which the sets $\Lambda_1 = \{(i\Delta, j\Delta) | 0 \le i \le M\ (h + 1) \le j \le N\}$, $\Lambda_2 = \{(i\Delta, j\Delta) | 0 \le i \le M\ s \le j \le h\}$, and $\Lambda_3 = \{(i\Delta, j\Delta) | 0 \le i \le M\ 0 \le j \le (s - 1)\}$ denote mesh points in the slab waveguide regions Ω_1, Ω_2, and Ω_3, respectively. As the empty circles shown in Fig. 2(b), we select the set of the mesh points $L_{12} = \{(i\Delta, j\Delta) | 0 \le i \le M\ j = h)\}$ as the interface between Λ_1 and Λ_2 and the set of the mesh points $L_{23} = \{(i\Delta, j\Delta) | 0 \le i \le$

$M\,j = s-1)\}$ as the interface between Λ_2 and Λ_3. The permittivity distribution of each slab waveguide is described by the notation $\varepsilon^m_{i,j} = \varepsilon(j\Delta,\, i\Delta) = \varepsilon_m(i\Delta),\ m = 1, 2, 3$.

Based on above definitions, we can define a discrete variation functional $J^m_{\text{rib-TM}}(E^m_{i,j}, \beta)$ associated with the functional (11) in each slab waveguide region Ω_m, as shown in (17), shown below. The objective is to find the extrema of the functional $J^m_{\text{rib-TM}}(E^m_{i,j}, \beta)$ in each slab waveguide region Λ_m subject to the Dirichlet's boundary condition (18), shown below, and the interface conditions (19) and (20), shown below:

$$\begin{aligned} J^m_{\text{rib-TM}}(E^m_{i,j}, \beta) &= \sum_{j\in\Lambda_m}\left\{\sum_{i=1}^{M-1}\varepsilon^m_{i,j}\left(E^m_{i,j} - E^m_{i,j-1}\right)^2 + \sum_{i=2}^{M-1}\varepsilon^m_{i,j}\left(E^m_{i,j} - E^m_{i-1,j}\right)^2 \right. \\ &\qquad \left. + \varepsilon^m_{1,j}\left(E^m_{1,j}\right)^2 + \varepsilon^m_{M,j}\left(E^m_{M-1,j}\right)^2 + \sum_{i=1}^{M-1} g^m_{i,j}(\beta)\left(E^m_{i,j}\right)^2\right\} \\ &= \sum_{j\in\Lambda_m}\left\{\left(u^m_j\right)^T\left(Q^m_j + G^m_j(\beta)\right)u^m_j + \left(u^m_j - u^m_{j-1}\right)^T D^m_j\left(u^m_j - u^m_{j-1}\right)\right\} \end{aligned} \tag{17}$$

$$(E^3_{i,0}) = 0 \tag{18}$$

$$E^1_{(i,j)\in L_{12}} = E^2_{(i,j)\in L_{12}}, \quad E^2_{(i,j)\in L_{23}} = E^3_{(i,j)\in L_{23}} \tag{19}$$

$$H^1_{(i,j)\in L_{12}} = H^2_{(i,j)\in L_{12}}, \quad H^2_{(i,j)\in L_{23}} = H^3_{(i,j)\in L_{23}}. \tag{20}$$

Note that we have applied Dirichlet's boundary condition $E^m_{0,j} = E^m_{M,j} = E^1_{i,N} = 0$, i.e., a discrete version of the boundary condition (12) into the functional (17). The boundary conditions (19) and (20) are discrete versions of the conditions (14)–(16). To solve the functional $J^m_{\text{rib-TM}}(E^m_{i,j}, \beta)$ by employing the dynamic programming technique, the functional $J^m_{\text{rib-TM}}(E^m_{i,j}, \beta)$ is expressed in an alternative matrix form in the second equality of (17), where the scalar coefficient $g^m_{i,j}(\beta)$, the $(M-1)\times 1$ column field u^m_j, and the $(M-1)\times(M-1)$ matrices D^m_j, Q^m_j, and $G^m_j(\beta)$ are given by

$$g^m_{i,j}(\beta) = \left(-\varepsilon^m_{i,j}\right)\left\{-\frac{1}{\left(\varepsilon^m_{i,j}\right)^2}\left(\frac{\varepsilon^m_{i+1,j} - \varepsilon^m_{i-1,j}}{2}\right)^2 + \frac{1}{\varepsilon^m_{i,j}}\left(\varepsilon^m_{i+1,j} + \varepsilon^m_{i-1,j} - 2\varepsilon^m_{i,j}\right) + \left(k_0^2\left(\varepsilon^m_{i,j}\right) - \beta^2\right)\Delta^2\right\}$$

$$u^m_j = \begin{pmatrix} E^m_{1,j} \\ E^m_{2,j} \\ \vdots \\ E^m_{M-1,j} \end{pmatrix}, \quad D^m_j = \text{diag}\begin{pmatrix} \varepsilon^m_{1,j} \\ \varepsilon^m_{2,j} \\ \vdots \\ \varepsilon^m_{M-1,j} \end{pmatrix}$$

$$Q^m_j = \left[\left(Q^m_j\right)_{p,q}\right] = \begin{cases} \varepsilon^m_{p,j} + \varepsilon^m_{p+1,j}, & p = q = 1, 2, \ldots (M-1), \\ -\varepsilon^m_{q,j}, & p - q = -1, \\ -\varepsilon^m_{p,j}, & p - q = +1, \\ 0, & \text{otherwise}, \end{cases} \qquad G^m_j(\beta) = \text{diag}\begin{pmatrix} g^m_{1,j}(\beta) \\ g^m_{2,j}(\beta) \\ \vdots \\ g^m_{M-1,j}(\beta) \end{pmatrix}. \tag{21}$$

3.2. Dynamic Programming Technique

Now we may use the dynamic programming procedure to evaluate the extrema of the functional $J^m_{\text{rib-TM}}(E^m_{i,j}, \beta)$. As shown in (22), shown below, and Fig. 2(b), we define $F^m_K(v, \beta), m = 1, 2, 3$ as solutions of the sub-problems associated with the waveguide problem (17), i.e., given a fixed value of

β, the function $F_K^m(v,\beta)$ is the extrema of the functional $J^m_{\text{rib-TM}}(E^m_{i,j},\beta)$ in the domain partitioning from $x = K$ to the rightmost edge of the slab waveguide region Λ_m

$$F_K^m(v,\beta)=\begin{cases}\min\limits_{u_K^1,u_{K+1}^1,\ldots u_N^1}\sum\limits_{j=K}^{N}\left\{\left(u_j^1\right)^T\left(Q_j^1+G_j^1(\beta)\right)u_j^1+\left(u_j^1-u_{j-1}^1\right)^T D_j^1\left(u_j^1-u_{j-1}^1\right)\right\}, & m=1\\ \min\limits_{u_K^2,u_{K+1}^2,\ldots u_h^2}\sum\limits_{j=K}^{h}\left\{\left(u_j^2\right)^T\left(Q_j^2+G_j^2(\beta)\right)u_j^2+\left(u_j^2-u_{j-1}^2\right)^T D_j^2\left(u_j^2-u_{j-1}^2\right)\right\}, & m=2\\ \min\limits_{u_K^3,u_{K+1}^3,\ldots u_{s-1}^3}\sum\limits_{j=K}^{s-1}\left\{\left(u_j^3\right)^T\left(Q_j^3+G_j^3(\beta)\right)u_j^3+\left(u_j^3-u_{j-1}^3\right)^T D_j^3\left(u_j^3-u_{j-1}^3\right)\right\}, & m=3.\end{cases}\tag{22}$$

By the same reasoning as (7) and (8) shown in the scalar mode theory, each function $F_K^m(v,\beta)$ in (22) can be written in an alternative recurrence form governing the function $F_K^m(v,\beta)$ and $F_{K+1}^m(v,\beta)$ in each slab waveguide region Λ_m can be derived:

In region Λ_1 :

$$F_K^1(v,\beta)=\min_{u_K^1}\left\{\left(u_K^1\right)^T\left(Q_K^1+G_K^1(\beta)\right)u_K^1+\left(u_K^1-v\right)^T D_K^1\left(u_K^1-v\right)+F_{K+1}^1\left(u_K^1,\beta\right)\right\}$$

$$(h+1)\le K\le(N-1)$$

$$F_N^1\left(u_{N-1}^1\right)=\left(u_N^1\right)^T\left(Q_N^1+G_N^1(\beta)\right)u_N^1+\left(u_N^1-u_{N-1}^1\right)^T D_N^1\left(u_N^1-u_{N-1}^1\right)=\left(u_{N-1}^1\right)^T D_N^1\left(u_{N-1}^1\right).$$

In region Λ_2 :

$$F_K^2(v,\beta)=\min_{u_K^2}\left\{\left(u_K^2\right)^T\left(Q_K^2+G_K^2(\beta)\right)u_K^2+\left(u_K^2-v\right)^T D_K^2\left(u_K^2-v\right)+F_{K+1}^2\left(u_K^2,\beta\right)\right\}$$

$$(s)\le K\le(h-1),$$

$$F_h^2\left(u_{h-1}^2,\beta\right)=\left(u_h^2\right)^T\left(Q_h^2+G_h^2(\beta)\right)u_h^2+\left(u_h^2-u_{h-1}^2\right)^T D_h^2\left(u_h^2-u_{h-1}^2\right)$$

In region Λ_3 :

$$F_K^3(v,\beta)=\min_{u_K^3}\left\{\left(u_K^3\right)^T\left(Q_K^3+G_K^3(\beta)\right)u_K^3+\left(u_K^3-v\right)^T D_K^3\left(u_K^3-v\right)+F_{K+1}^3\left(u_K^3,\beta\right)\right\}$$

$$1\le K\le(s-2)$$

$$F_{s-1}^3\left(u_{s-2}^3,\beta\right)=\left(u_{s-1}^3\right)^T\left(Q_{s-1}^3+G_{s-1}^3(\beta)\right)u_{s-1}^3+\left(u_{s-1}^3-u_{s-2}^3\right)^T D_{s-1}^3\left(u_{s-1}^3-u_{s-2}^3\right)\tag{23}$$

where $v=u_{K-1}^m$ in the functions $F_K^m(v,\beta), m=1,2,3$. Given the functions $F_N^1(u_{N-1}^1)$, $F_h^2(u_{h-1}^2,\beta)$, and $F_{s-1}^3(u_{s-2}^3,\beta)$ at the right edge of each slab waveguide region $\Lambda_m, m=1,2,3$, as shown in Fig. 2(b), the function at the left edge of each slab waveguide region $\Lambda_m, m=1,2,3$, i.e., $F_{h+1}^1(v,\beta)=\min_{u_{h+1}^1,u_{h+2}^1,\ldots u_N^1}\{J^1_{\text{rib-TM}}(E^1_{i,j},\beta)\}$, $F_s^2(v,\beta)=\min_{u_s^2,u_{s+1}^2,\ldots u_{h-1}^2}\{J^2_{\text{rib-TM}}(E^2_{i,j},\beta)\}$, and $F_1^3(v,\beta)=\min_{u_1^3,u_2^3,\ldots u_{s-2}^3}\{J^3_{\text{rib-TM}}(E^3_{i,j},\beta)\}$, i.e., the extrema of the functional $J^m_{\text{rib-TM}}(E^m_{i,j},\beta)$ shown in (17) in each slab waveguide region $\Lambda_m, m=1,2,3$ can be derived by recursively minimizing (23).

Based on the observation from (23) that all of the initial functions $F_N^1(u_{N-1}^1)$, $F_h^2(u_{h-1}^2,\beta)$, and $F_{s-1}^3(u_{s-2}^3,\beta)$ have the quadratic form, we assume the functions $F_K^m(v,\beta), m=1,2,3$ inherits the quadratic characteristic so that we can express the functions $F_K^m(v,\beta), m=1,2,3$ in terms of the $(M-1)\times(M-1)$ unknown coefficient matrices $A_K^m(\beta)$, $B_K^m(\beta)$, and unknown scalar function $W_K^m(\beta)$ as

$$F_K^m(v,\beta)=\begin{cases}v^T\left(D_K^1\right)^T A_K^1(\beta)v, & m=1\\ v^T\left(D_K^2\right)^T A_K^2(\beta)v-2\cdot v^T\left(D_K^2\right)^T B_K^2(\beta)\left(u_h^2\right)+W_K^2(\beta), & m=2\\ v^T\left(D_K^3\right)^T A_K^3(\beta)v-2\cdot v^T\left(D_K^3\right)^T B_K^3(\beta)\left(u_{s-1}^2\right)+W_K^3(\beta), & m=3.\end{cases}\tag{24}$$

By substituting the quadratic expression (24) for each $F_K^m(v,\beta)$ into the recurrence equation (23) and algebraically carrying out the essential quadratic optimization over the field u_K^m, the iterative relations for the $(M-1)\times(M-1)$ coefficient matrices $A_K^m(\beta)$, $B_K^m(\beta)$ and the iterative relation for the $(M-1)\times 1$ column field u_K^m in each region Λ_m can be derived:

$$A_K^m(\beta) = I - \left(D_K^m + Q_K^m + G_K^m(\beta) + \left(D_{K+1}^m\right)^T A_{K+1}^m(\beta)\right)^{-1}\left(D_K^m\right), \qquad K \in \Lambda_m, \quad m = 1,2,3$$

$$A_N^1 = I, \quad A_h^2 = I, \quad A_{s-1}^3 = I$$

$$B_K^m(\beta) = \left(I - A_K^m(\beta)\right)B_{K+1}^m(\beta), \qquad K \in \Lambda_m, \quad m = 2,3$$

$$B_h^2 = I, \quad B_{s-1}^3 = I$$

$$u_K^m = \begin{cases} \left(I - A_K^1(\beta)\right)\left(u_{K-1}^1\right), & m = 1,\ (h+1) \le K \le (N-1) \\ \left(I - A_K^2(\beta)\right)\left(u_{K-1}^2\right) + B_K^2(\beta)\left(u_h^2\right), & m = 2,\ (s) \le K \le (h-1) \\ \left(I - A_K^3(\beta)\right)\left(u_{K-1}^3\right) + B_K^3(\beta)\left(u_{s-1}^3\right), & m = 3,\ 1 \le K \le (s-2). \end{cases} \tag{25}$$

The iterative relation for the field u_K^m in each slab waveguide region Λ_m can be connected via considering the field continuities at the interfaces between the slab waveguide regions, i.e., the conditions shown in (19) and (20). In the discrete variational model shown in (17)–(21), the field u_K^m defined in (21) naturally satisfies the condition (19), i.e., $u_h^2 = E_{(i,j)\in L_{12}}^1 = E_{(i,j)\in L_{12}}^2$, and $u_{s-1}^3 = E_{(i,j)\in L_{23}}^2 = E_{(i,j)\in L_{23}}^3$. Meanwhile, the magnetic fields at the interfaces of the slab waveguide regions can be derived by employing the finite-difference method on the wave equation (10) in order to express the first derivative of the electric modal field at the interfaces of the slab waveguide region, i.e., $\partial E_y^1(x=\ell_{12},y)/\partial x$, $\partial E_y^2(x=\ell_{12},y)/\partial x$, $\partial E_y^2(x=\ell_{23},y)/\partial x$, and $\partial E_y^3(x=\ell_{23},y)/\partial x$, which are shown in (15) and (16) in terms of the discrete modal fields u_{h+1}^1, u_h^2, u_{h-1}^2, u_s^2, u_{s-1}^3, and u_{s-2}^3:

$$\frac{\partial E_y^1(x=\ell_{12},y)}{\partial x} = \frac{1}{(2\Delta)}\left\{\left\{P_1 + \frac{1}{4}Q_1\left(\varepsilon_{i,h}^2\right)\cdot P_2 - \left[2 + (\Delta\cdot\beta)^2\right] \cdot I + Q_2\left(\varepsilon_{i,h}^2\right) + (\Delta\cdot k_0)^2 Q_3\left(\varepsilon_{i,h}^2\right)\right\}u_h^2 + 2u_{h+1}^1\right\}$$

$$\frac{\partial E_y^2(x=\ell_{12},y)}{\partial x} = \frac{(-1)}{(2\Delta)}\left\{\left\{P_1 + \frac{1}{4}Q_1\left(\varepsilon_{i,h}^2\right)\cdot P_2 - \left[2 + (\Delta\cdot\beta)^2\right] \cdot I + Q_2\left(\varepsilon_{i,h}^2\right) + (\Delta\cdot k_0)^2 Q_3\left(\varepsilon_{i,h}^2\right)\right\}u_h^2 - 2u_{h-1}^2\right\}$$

$$\frac{\partial E_y^2(x=\ell_{23},y)}{\partial x} = \frac{1}{(2\Delta)}\left\{\left\{P_1 + \frac{1}{4}Q_1(\varepsilon_{i,s-1}^3)\cdot P_2 - \left[2 + (\Delta\cdot\beta)^2\right] \cdot I + Q_2\left(\varepsilon_{i,s-1}^3\right) + (\Delta\cdot k_0)^2 Q_3\left(\varepsilon_{i,s-1}^3\right)\right\}u_{s-1}^3 + 2u_s^2\right\}$$

$$\frac{\partial E_y^3(x=\ell_{23},y)}{\partial x} = \frac{(-1)}{(2\Delta)}\left\{\left\{P_1 + \frac{1}{4}Q_1\left(\varepsilon_{i,s-1}^3\right)\cdot P_2 - \left[2 + (\Delta\cdot\beta)^2\right] \cdot I + Q_2\left(\varepsilon_{i,s-1}^3\right) + (\Delta\cdot k_0)^2 Q_3\left(\varepsilon_{i,s-1}^3\right)\right\}u_{s-1}^3 - 2u_{s-2}^3\right\} \tag{26}$$

where the $(M-1)\times(M-1)$ constant matrices P_1, P_2, and the $(M-1)\times(M-1)$ matrices $Q_1(\cdot)$, $Q_2(\cdot)$, $Q_3(\cdot)$, which are the functions of the dielectric constants $\varepsilon_{i,h}^2$ and $\varepsilon_{i,s-1}^3$ at the mesh

points $L_{12}=\{(i\Delta, j\Delta)|0\le i\le M\ j=h)\}$ and $L_{23}=\{(i\Delta, j\Delta)|0\le i\le M\ j=s-1)\}$ are given by

$$P_1=\left[(P_1)_{p,q}\right]=\begin{cases}-2, & p=q\\ 1, & |p-q|=1,\\ 0, & \text{otherwise}\end{cases}\quad P_2=\left[(P_2)_{p,q}\right]=\begin{cases}1, & p-q=-1\\ -1, & p-q=+1\\ 0, & \text{otherwise}\end{cases}$$

$$Q_1\left(\varepsilon_{i,j}^m\right)=\text{diag}\left\{\frac{1}{\varepsilon_{i,j}^m}\left(\varepsilon_{i+1}^m-\varepsilon_{i-1}^m\right)\right\},\qquad 1\le i\le(M-1),\quad j=h,(s-1),\quad m=2,3$$

$$Q_2\left(\varepsilon_{i,j}^m\right)=\text{diag}\left\{-\frac{1}{\left(\varepsilon_{i,j}^m\right)^2}\left(\frac{\varepsilon_{i+1,j}^m-\varepsilon_{i-1,j}^m}{2}\right)^2+\frac{1}{\varepsilon_{i,j}^m}\left(\varepsilon_{i+1,j}^m+\varepsilon_{i-1,j}^m-2\varepsilon_{i,j}^m\right)\right\}$$

$$Q_3\left(\varepsilon_{i,j}^m\right)=\text{diag}\left\{\varepsilon_{i,j}^m\right\}. \tag{27}$$

By substituting the expressions of the magnetic modal fields shown in the equation (26) into the conditions (20), we derive two auxiliary equations which illustrates the iterations of the modal fields u_K^m at the interfaces of the slab waveguide regions, i.e., $K=h$ and $K=s-1$:

$$\begin{aligned}u_{h+1}^1&=a_h u_h^2+b_h u_{h-1}^2\\ u_s^2&=a_{s-1}u_{s-1}^3+b_{s-1}u_{s-2}^3\\ a_j&=\begin{cases}(-1)\left\{P_1+\frac{1}{4}Q_1\left(\varepsilon_{i,h}^2\right)\cdot P_2-\left[2+(\Delta\cdot\beta)^2\right]\cdot I+Q_2\left(\varepsilon_{i,h}^2\right)+(\Delta\cdot k_0)^2Q_3\left(\varepsilon_{i,h}^2\right)\right\}, & j=h\\ (-1)\left\{P_1+\frac{1}{4}Q_1\left(\varepsilon_{i,s-1}^3\right)\cdot P_2-\left[2+(\Delta\cdot\beta)^2\right]\cdot I+Q_2\left(\varepsilon_{i,s-1}^3\right)+(\Delta\cdot k_0)^2Q_3\left(\varepsilon_{i,s-1}^3\right)\right\}, & j=(s-1)\end{cases}\\ b_j&=-1,\quad j=h,\ (s-1).\end{aligned} \tag{28}$$

With the use of the above equations, the dependence of u_h^2 or u_{s-1}^3 for the modal field iterations (25) in the slab waveguide regions Λ_2 and Λ_3 can be eliminated and then an equivalent model which illustrates the modal field iteration in the overall mesh $\Lambda=\Lambda_1\cup\Lambda_2\cup\Lambda_3$ can be characterized by the corresponding coefficient matrices $C_K^{equiv.}(\beta)$:

$$u_K^m=\left(I-C_K^{equiv.}(\beta)\right)u_{K-1}^m,\ 1\le K\le(N-1),\ m=1,2,3$$

$$C_K^{equiv.}(\beta)=\begin{cases}A_K^1(\beta), & (h+1)\le K\le(N-1)\\ I+\left(a_h-I+A_{h+1}^1(\beta)\right)^{-1}(b_h), & K=h\\ I-\left\{I+B_K^2(\beta)\cdot\left[B_{K+1}^2(\beta)\right]^{-1}\right.\\ \qquad\left.\times\left(C_{K+1}^{equiv.}(\beta)-A_{K+1}^2(\beta)\right)\right\}^{-1}(I-A_K^2(\beta)), & (s)\le K\le(h-1)\\ I+\left(a_{s-1}-I+A_s^2(\beta)\right)^{-1}(b_{s-1}), & K=(s-1)\\ I-\left\{I+B_K^3(\beta)\cdot\left[B_{K+1}^3(\beta)\right]^{-1}\right.\\ \qquad\left.\times\left(C_{K+1}^{equiv.}(\beta)-A_{K+1}^3(\beta)\right)\right\}^{-1}(I-A_K^3(\beta)), & 1\le K\le(s-2)\end{cases} \tag{29}$$

where $C_N^{equiv.}(\beta)=I$ followed by the observation $C_N^{equiv.}(\beta)=A_N^1=I$ in (25). The iterative relation for modal field u_0^3 and u_1^3 can be written as $(I-C_1^{equiv.}(\beta))^{-1}u_1^3=u_0^3=0$, as followed by applying the Dirichlet's boundary condition (18), i.e., $u_0^3=(E_{i,0}^3)=0$. Based on this equation, the variational quasi-TM mode problem shown in (11)–(16) can be solved by evaluating the $(M-1)\times(M-1)$ coefficient matrix $C_1^{equiv.}(\beta)$ in the first place. Then the exact value of the propagation

constant β can be derived by solving the equation $\det[(I - C_1^{equiv.}(\beta))^{-1}] = 0$. Once the final value of β has been determined, the modal field u_1^3 can be derived by solving the linear equation $(I - C_1^{equiv.}(\beta))^{-1} u_1^3 = 0$. Finally, the other modal fields u_K^m for $K = 2, \ldots, (N-1)$ can be derived by employing (29).

4. Comparison in Algorithmic Performance to EIM, FDM, and FEM

The strategy used to solve the quasi-TM modal field in this paper, i.e., partition the original rib-type waveguide structure into three slab waveguide regions in the first place, then solves the part of the modal filed $E_y^m((x, y) \in \Omega_m)$ in each slab waveguide region, and finally combines them into the modal field defined in the entire computational window, is distinct from the one used in the effective index method (EIM) [16], [22]. In case of the rib-type dielectric waveguide, EIM assumes the modal field solution has the form of the separation of the variables, and thus the original rib-type waveguide problem can be transformed into two slab waveguide problems along the x-direction and the y-direction, respectively. However, such assumption causes EIM actually analyzes the separable permittivity distribution, which differs from the original permittivity distribution $\varepsilon(x, y)$ in the computational window [16]. Such an error in the permittivity distribution substantially deteriorates the numerical accuracy in the evaluation of β, especially in the case of the strongly guiding, rib-type waveguide [16]. On the other hand, The numerical calculation in Section 5 demonstrates that the quasi-TM method proposed in this paper, accurately solves the local field $E_y^m((x, y) \in \Omega_m)$ in each slab waveguide region, and then combines them into the accurate modal field solution existable in the original permittivity distribution $\varepsilon(x, y)$. Therefore compared to EIM, the partitioning strategy used in this paper exhibits no error in the evaluation of the modal field, and thus the modal indices β.

Meanwhile, we may compare the time complexity of the proposed mode solver with those of finite difference method (FDM) and finite element method (FEM) by evaluating the number of the dominant matrix operations. Here we assume that these mode solvers use a common algorithm, e.g., Gauss-Jordan method to carry out the dominant matrix operations. Then in the case of the rectangular computational window, the total number of the mesh points determines the number of the dominant matrix operations required by these mode solvers. For instance, the proposed scalar mode solver (9) illustrates that, given a fixed computational window size $\Omega = L_x \times L_y$ shown in Fig. 1, the corresponding the number of the mesh points $(M+1) \times (N+1)$ determines the computational cost to carry out the matrix inverse operations until the coefficient matrix $C_1(\beta)$ in the nonlinear equation $\det[(I - C_1(\beta))^{-1}] = 0$ is derived. If FDM or FEM is used to solve the waveguide problem within the computational window $\Omega = L_x \times L_y$, we assume that Gauss–Jordan algorithm is used to diagonalize the resultant eigen-value matrix whose size is also the function of the total number of the mesh points or the total number of the mesh elements.

Moreover, in the common case, given a fixed computational window size $\Omega = L_x \times L_y$, all of the above three mode solvers require a moderate to large number of the mesh points in order to derive the convergent modal indices. That is, in the condition of the convergence of the modal calculation, we can fairly evaluate the number of the dominant matrix operations required by these mode solvers in terms of the Big-O notation as the function of the number of the mesh points or the number of the mesh elements.

To evaluate the time complexity of the FDM, first, as shown in Fig. 1(b), it can be observed that given a fixed computational window size $\Omega = L_x \times L_y$, there requires $(M-1) \times (N-1)$ unknowns to describe the modal field within the boundary of the computational window, because the modal field at the boundary points has been designated by the boundary condition. If we apply FDM to calculate the modal indices and the modal field of the waveguide structure in Fig. 1(b), there requires $O((N-1)^3(M-1)^3)$ matrix operations in order to compute the diagonalization of the resulting eigen-value matrix.

In the FEM case, if the same computational window $\Omega = L_x \times L_y$ shown in Fig. 1(a) is divided into M_e elements, each of which is described by N_e nodes, there requires $O((N_e)^3(M_e)^3)$ matrix

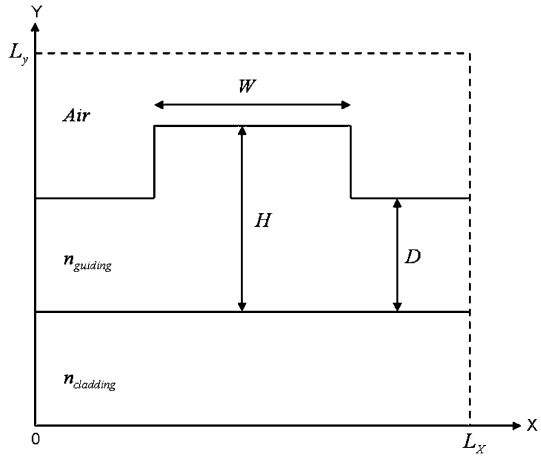

Fig. 3. A rib-type rectangular waveguide for numerical demonstration in this study.

operations in order to compute the diagonalization of the resulting eigen-value matrix. Therefore it can be evaluated that in order to derive all convergent modal indices, FDM or FEM requires the number of the dominant matrix operations which is about the sixth power of the amount of the input data, i.e., $(N-1)^3(M-1)^3$ in the FDM case and $(N_e)^3(M_e)^3$ in the FEM case. Note that the above evaluation of the number of the dominant matrix operations required by FDM or FEM is obtained by treating the resultant eigen-value matrices as fully dense. In fact, the sparsity of the eigen-value matrix for FEM is highly associated with the order of the shape functions. A highly sparse eigen-value matrix can be achieved by decreasing the order of the shape function. Meanwhile, there indeed exists several other algorithms to diagonalize such sparse eigen-value matrix more efficiently. However, decreasing the order of the shape function may deteriorate the accuracy of the modal calculations.

Compared to FDM and FEM, the dominant matrix operations for the proposed scalar mode solver (9) can be evaluated to be $O((n_\beta)(N-1)(M-1)^3)$, where n_β is the factor representing the number of the Newton's like steps required to derive all modal indices in the nonlinear equation $\det[(I-C_1(\beta))^{-1}]=0$. That is, the single-mode or few-modes waveguide structure leads to the small factor n_β. The corresponding time complexity of the proposed scalar mode solver (9) is about the fourth power of the amount of the input data, i.e., $(N-1)(M-1)^3$. However, in the case of the multi-mode waveguide structure, to calculate all modal indices the required number of the dominant matrix operations for the proposed mode solver (9) grows with the factor n_β.

We can evaluate the space complexity of any of the above mode solvers as the storage size required by the mode solver in order to calculate one modal index. Note that the proposed scalar mode solver (9) shows that the modal indices can be derived via the calculation of the solution of the equation $\det[(I-C_1(\beta))^{-1}]=0$, which simply involves the coefficient matrix $C_1(\beta)$. Equation (9) shows that the matrix $C_1(\beta)$ can derived by sequentially evaluating each coefficient matrix $C_K(\beta)$ from the given matrix $C_N(\beta)=I$. This process implies that the proposed scalar mode solver simply requires a common memory space to sequentially store $(M-1)\times(M-1)$ matrix $C_K(\beta)$ during the program execution. However, FDM or FEM requires a larger memory space to store the eigen-value matrix with its size as large as $(M-1)(N-1)\times(M-1)(N-1)$ in the FDM case or $M_eN_e\times M_eN_e$ in the FEM case during the computation of the matrix diagonalization. Thus the proposed method also improves the space efficiency by preventing the diagonalization of large matrix.

5. Numerical Results and Discussion

We numerically investigate the accuracy and the efficiency of the proposed method via the calculation of the scalar and quasi-TM, guided modes in two rib-type, dielectric waveguides. The

TABLE 1

Scalar mode indices calculated by the proposed method, BeamPROP and the variational Fourier transform method [24] for the GaAs-on-AlGaAs, rib-type waveguide. Relative error between the proposed method and the variational Fourier transform method [24] is $(3.4137327 - 3.41377096)/3.41372428 = 1.12 \times 10^{-5}$. Relative error between the proposed method and BeamPROP is $(3.413730 - 3.41377096)/3.41377096 = 1.2 \times 10^{-5}$

Proposed method (scalar mode)			BeamPROP $D = 0.6\mu m$, $\Delta z = 0.1\mu m$			Ref. [24]
Mesh size (M+1)×(N+1)	n_{eff}	CPU (sec.)	Mesh size (M+1)×(N+1)	n_{eff}	CPU (sec.)	n_{eff}
51×201	3.41441214	0.078	41×161	3.413524	2.35	3.4137327
61×241	3.41429522	0.187	81×321	3.413644	4.28	
71×281	3.41405815	0.281	101×401	3.413665	7.10	
81×321	3.41398778	0.359	201×801	3.413703	24.31	
91×361	3.41384823	0.516	223×889	3.413730	30.28	
101×401	3.41380325	0.765				
111×441	3.41377096	0.843				

cross section of the rib waveguide shown in Fig. 3 represents the computational window $\Omega = L_x \times L_y$ for modal calculation. In this window, the rib width, the rib height, and the slab thickness are denoted as W, H, and D respectively. Both waveguides have an air cap, and the refractive indices $n_{guiding}$ and $n_{cladding}$ in the guiding layer and the cladding layer, respectively. The first type of the rib waveguides is designated as a weakly-guiding, GaAs-on-AlGaAs heterostructure with the refractive indices $n_{guiding} = 3.44$ and $n_{cladding} = 3.4$ at 1.15 μm. The waveguide appears to have a large cross section and have a single guided mode. The geometric parameters designated are consistent with those shown in [24], i.e., $W = 3$ μm, $H = 1$ μm, and $D = 0.6$ μm. The second type of the rib waveguides is designated as a strongly guiding, silicon-on-insulator (SOI) heterostructure with the refractive indices $n_{guiding} = 3.44$ and $n_{cladding} = 1.46$ at 1.55 μm. The geometric parameters are appropriately designated in order to satisfy the single guided mode condition presented by Soref *et al.* [25]. The resulting rib waveguide also has a large cross section with $W = H = 5$ μm, and $D = 4$ μm. These two waveguides will be numerically analyzed by employing the proposed method and the commercial simulator BeamPROP, respectively. Here the numerical results derived via the BeamPROP are considered as a benchmark to compare with the results obtained by the proposed method. The accuracy of the proposed method is evaluated in terms of the relative error. Moreover, in the same computational environment, we evaluate the efficiency of the proposed method by comparing the CPU times spent by the proposed method and the BeamPROP.

To evaluate the scalar mode indices for the first type, weakly guiding GaAs-on-AlGaAs waveguide, it is realized that the mesh grid size Δ, which involves the discretization approximation of the first derivatives of the modal field $E(x, y)$ in the variation functional $J(E(x, y), \beta)$ in (5) affects the numerical accuracy of the modal calculation. In the numerical experiment, the computational window size is fixed to $\Omega = L_x \times L_y = 8 \times 2$ $(\mu\text{m})^2$. Then the proposed method (9) is used to calculate the scalar mode indices for the mesh grid size Δ varied from 0.04 μm (51 $\times$ 201 mesh points) to 0.0182 μm (111 $\times$ 441 mesh points), in order to determine the convergent mode index. Table 1 shows the scalar mode indices n_{eff} calculated by using the proposed method (9), the variational Fourier transform method [24], and the simulator BeamPROP. It shows that the proposed method (9) with grid size $\Delta = 0.0182$ μm gives a convergent index.

The calculated modal index values converge to 3.41377096, which is almost consistent to the convergent index value derived by the variational Fourier transform method [24] or the BeamPROP, respectively. The relative error between the modal indices calculated by the proposed method and the other two methods reaches 10^{-5} in the convergence case.

Table 1 also shows that the CPU time of about 0.843 sec is spent by the proposed method in order to derive fundamental mode index whose relative error reaches 10^{-5}. Compared to the CPU time spent by BeamPROP, the proposed method spends much less CPU time to reach the convergence of the modal calculation. The reason resulting in such an improvement in the algorithmic efficiency can be explained as follows.

When the proposed method is utilized to calculate the scalar mode indices in the waveguide structure in Fig. 3, the main computational burden comes from two sources. First, the dominant matrix operations based on the sequential calculation of the coefficient matrices $C_K(\beta)$ from $K = N - 1$ to $K = 1$ must be carried out in order to derive the coefficient matrix $C_1(\beta)$ in the nonlinear equation $\det[(I - C_1(\beta))^{-1}] = 0$. Equation (9) shows that the calculation of each coefficient matrix $C_K(\beta)$ involves the inverse of a $(M-1) \times (M-1)$ matrix $I + Q + G_K(\beta) + C_{K+1}(\beta)$. Second, once the coefficient matrix $C_1(\beta)$ has been derived, there still requires an additional computation work to find the roots β of the nonlinear equation $\det[(I - C_1(\beta))^{-1}] = 0$.

Regarding the first source, if the matrix inversion takes place in terms of Gauss-Jordan elimination process, there totally requires $O((N-1)(M-1)^3)$ multiplications to invert all matrices $I + Q + G_K(\beta) + C_{K+1}(\beta)$, $K = 1, 2, \ldots, (N-1)$. The bottleneck term $(M-1)^3$ is not considered as an issue because it can be seen from the equation (9) that the dimension of each matrix $I + Q + G_K(\beta) + C_{K+1}(\beta)$ to be inverted is $(M-1) \times (M-1)$ associated with the amount of the mesh points along y-direction in Fig. 1(b). For the weakly guiding, GaAs-on-AlGaAs, rib-type waveguide with an air cap, there exists a high refractive index contrast between the GaAs rib and the air. The guided mode field at the top of the rib has an evanescent tail that extends a very short distance into the air. That is, there requires few mesh points to describe this evanescent tail that extends from the top of the rib to the edge $y = L_y$ of the computational window Ω.

Table 1 illustrates the connection between the dimension of each matrix $I + Q + G_K(\beta) + C_{K+1}(\beta)$ to be inverted and the efficiency of the proposed method in the scalar mode calculation for weakly guiding waveguide. By using the matrices $I + Q + G_K(\beta) + C_{K+1}(\beta)$ with small size, e.g., about 99 $\times$ 99 in (9) to calculate each coefficient matrix $C_K(\beta)$, the scalar mode index calculated by the proposed method can reach a high degree of precision, i.e., to the relative error of 10^{-5} within 1 second. In fact, for each K, $K = 1, 2, \ldots, (N-1)$, the symmetric matrix $I + Q + G_K(\beta)$ in (9) can be made to be positively definite by appropriately choosing the mesh grid size Δ. Then based on the symmetric, positive definite matrix $C_N(\beta) = I$ at the initial step $K = N$, the matrix $I + Q + G_K(\beta) + C_{K+1}(\beta)$ at the other steps K in (9) can be symmetric and positively definite. To invert such matrices there exists a more efficient algorithm, e.g., Cholesky based factorization algorithm.

Regarding the second source impacting on the efficiency of the scalar mode calculation, it involves the additional computation work to search the roots of the nonlinear equation $\det[(I - C_1(\beta))^{-1}] = 0$. In this paper a Newton-like algorithm is used to search the roots, and we have characterized the computational work to search all roots of the nonlinear equation by the factor n_β in Section 4. Although the efficiency of such an algorithm significantly depends with the initial guess to the value of β, the experimental result shows that the convergence to an accurate solution of the nonlinear equation $\det[(I - C_1(\beta))^{-1}] = 0$ is obtainable within a few iteration steps if the initial value of β is suitably selected as the starting point.

To investigate the quasi-TM mode properties in the first type, weakly guiding GaAs-on-AlGaAs waveguide, first, (29) is used to calculate the corresponding modal indices. Table 2 shows the modal indices n_{eff} calculated by the proposed quasi-TM method (29), the variational Fourier transform method [24], and the simulator BeamPROP. It shows that the proposed quasi-TM method (29) with the grid size $\Delta = 0.02$ μm (101 $\times$ 401 mesh points) gives a convergent

TABLE 2

Quasi-TM mode indices calculated by the proposed method, BeamPROP and the variational Fourier transform method [24] for the GaAs-on-AlGaAs rib-type waveguide. Relative error between the proposed method and the variational Fourier transform method [24] is $(3.41209251 - 3.4119530)/3.4119530 = 4.09 \times 10^{-5}$. Relative error between the proposed method and BeamPROP is $(3.41209251 - 3.411971)/3.411971 = 3.56 \times 10^{-5}$

Proposed method (quasi-TM mode)			BeamPROP $D = 0.6\mu m$, $\Delta z = 0.1\mu m$			Ref. [24]
Mesh size (M+1)×(N+1)	n_{eff}	CPU (sec.)	Mesh size (M+1)×(N+1)	n_{eff}	CPU (sec.)	n_{eff}
51×201	3.41310682	0.251	26×101	3.411790	2.05	3.4119530
61×241	3.41274802	0.462	41×161	3.411842	3.11	
71×281	3.41254107	0.767	81×321	3.411939	7.70	
81×321	3.41233807	1.022	101×401	3.411952	11.28	
91×361	3.41222402	1.363	201×801	3.411971	41.55	
101×401	3.41209251	2.090				
111×441	3.41202330	3.044				

mode index. The modal index values calculated by the proposed algorithm converge to 3.41209251, which is in good agreement with the convergent index value n_{eff} reported in [24] and that obtained by BeamPROP. The relative error between the modal indices calculated by the proposed method and the other two methods reaches 10^{-5} in the convergence case.

The proposed quasi-TM method in Section 3 shows that in addition to the approximation of the first derivatives of the modal fields in the discretization of the variation functional (11), the derivation of the auxiliary equation (28) for the purpose of the magnetic field matching (20) involves the approximation of the second derivatives of the modal fields at the interfaces $j = h$ and $j = s - 1$, as described by (26) and (27). It might cause the numerical inaccuracy in the calculation of the modal indices. However, the calculated results shown in Table 2 illustrate that the convergent mode index is accurate so it can be inferred that the error caused by the discretization of second derivatives of the modal fields in (26) and (27) would not be magnified and propagate toward the coefficient matrix $C_1^{equiv.}(\beta)$ during the sequential calculation of the coefficient matrices $C_K^{equiv.}(\beta)$, $K = 1, 2, \ldots, (N-1)$.

Table 2 shows that the proposed method spends 2.090 sec. to derive a convergent, quasi-TM mode index whose relative error reaches 10^{-5}. Given a fixed computational window size $\Omega = L_x \times L_y = 8 \times 2\ (\mu\ \mathrm{m})^2$, and a fixed mesh size $(M+1) \times (N+1) = 101 \times 401$, BeamPROP spends much more CPU time, i.e., 11.28 sec. to reach the convergence of the modal calculation.

To verify the accuracy in the calculation of the corresponding modal field profile, we plot the contour of the quasi-TM modal field based on (29). Fig. 4(a) shows the resulting contour at the field levels of 10% to 90% of the maximum at an interval of 10%. The resulting field contour in Fig. 4(a) is in good agreement with the one shown in Fig. 4(b), which is obtained by using BeamPROP.

We apply the scalar mode method (9) and the quasi-TM mode method (29) to calculate the modal indices and the corresponding modal fields for the strongly guiding, silicon-on-insulator, rib-type dielectric waveguide, as shown in Fig. 3. As indicated by Soref *et al.* in [25], SOI based rib waveguide with a cross section of several microns is allowed to have single- guided mode

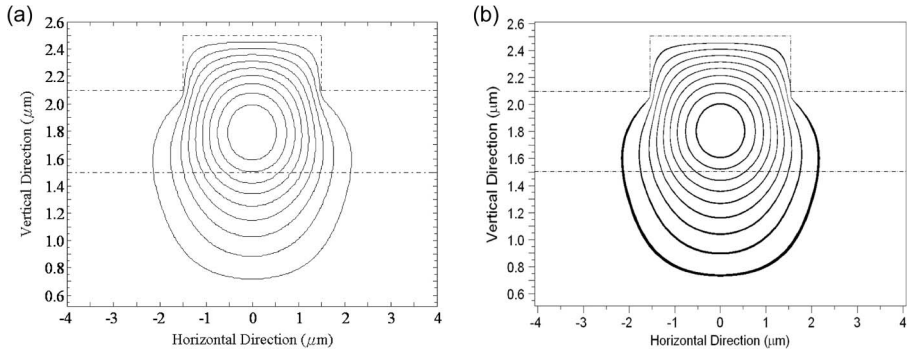

Fig. 4. Quasi-TM mode contour with field levels at 10% to 90% of the maximum at an interval of 10% obtained by (a) the proposed method (101 × 401 points) and (b) BeamPROP.

only when the ratio of the rib width to rib height satisfies Soref's single-mode condition [25]. By using the notations defined in Fig. 3, the SOI waveguide has a rib size of $W = H = 5$ μm, and a slab thickness of $D = 4$ μm. The corresponding ratio of the rib width to the rib height W/H satisfies Soref's single mode condition. In the numerical calculation, given a fixed computational window size $\Omega = L_x \times L_y = 10 \times 6$ $(\mu\text{m})^2$, the proposed methods (9) and (29) are used to calculate the mode indices for the mesh grid size Δ varied from 0.6 μm (11 × 18 mesh points) to 0.05 μm (121 × 201 mesh points), in order to determine the convergent mode index. Table 3 shows the scalar and quasi-TM mode indices n_{eff} calculated by using the proposed methods, and the simulator BeamPROP.

Table 3 shows that both scalar mode method (9) and quasi-TM mode method (29) with the same grid size $\Delta = 0.12$ μm (51 × 84 mesh points) give convergent indices. The scalar and quasi-TM mode index values calculated by the proposed methods converge to 3.435536056 and 3.435337612, respectively, both of which are almost consistent to the convergent mode index values calculated by the BeamPROP. The relative error between the convergent mode indices calculated by the proposed methods and the BeamPROP reaches 10^{-6} in the convergence case. Table 3 also shows a fact that for high index contrast waveguide, e.g., the SOI waveguide mentioned here, the minimum size of the coefficient matrices, i.e., $C_K(\beta)$ or $C_K^{equiv.}(\beta)$ required to derive a convergent mode index is about 49 × 49. That is, in the case of SOI waveguide, the dominant matrix operations required by the proposed methods (9) or (29) simply involve the inverse of the small matrices. Thus Table 3 demonstrates that the proposed methods have the capability to calculate the accurate modal indices of the SOI waveguide in an efficient fashion.

Table 3 shows the proposed scalar and quasi-TM mode methods spend 0.032 sec. and 0.109 sec., respectively, to derive convergent mode indices. Given the same computational window size $\Omega = L_x \times L_y = 10 \times 6$ $(\mu\text{m})^2$, and mesh size $(M+1) \times (N+1) = 51 \times 84$, BeamPROP spends much more CPU time, i.e., 4.61 sec. and 5.55 sec., respectively, to derive convergent mode indices instead.

Finally, to verify the accuracy in the calculation of the guided mode profile of the SOI waveguide, we plot the contour of the scalar mode field based on the field iteration equation (9). Fig. 5(a) shows the resulting field contour at the field levels of 10% to 90% of the maximum at an interval of 10%. The resulting field contour in Fig. 5(a) is in good agreement with the one shown in Fig. 5(b), which is obtained by using BeamPROP.

The previous two examples show that the quasi-TM mode method (29) is applicable to calculate the modal indices and the modal field contours for both weakly and strongly guiding, rib-type dielectric waveguides. In fact, the quasi-TM mode method (29) can be suitably modified to investigate the modal properties of the plasmonic waveguides. Here we apply the modified method to calculate the hybrid guided field contour for a rib-type, conductor-gap-silicon (CGS) plasmonic waveguide [26]. The schematic description of the CGS plasmonic waveguide is

TABLE 3

(a) Scalar modal indices calculated by the proposed method and BeamPROP for the strongly guiding, silicon-on-insulator rib-type waveguide shown in Fig. 3. Relative error is $(3.435536056 - 3.435585)/3.435585 = -1.42 \times 10^{-5}$. (b) Quasi-TM modal indices calculated by the proposed method and the BeamPROP for the same waveguide. Relative error is $(3.435337612 - 3.435360)/3.435360 = -6.52 \times 10^{-6}$

(a)

Proposed method (scalar mode)			BeamPROP		
Mesh size (M+1)×(N+1)	n_{eff}	CPU (sec.)	Mesh size (M+1)×(N+1)	n_{eff}	CPU (sec.)
11×18	3.436717888	<<0.01	11×18	3.437374	1.03
21×34	3.435895392	<<0.01	21×34	3.435798	1.45
31×51	3.435814796	<<0.01	31×51	3.435830	2.33
41×68	3.435773364	0.0162	41×68	3.435522	3.10
51×84	3.435536056	0.032	51×84	3.435585	4.61
61×101	3.435567188	0.062	61×101	3.435573	5.90
71×118	3.435589368	0.109	71×118	3.435604	7.26
81×134	3.435451084	0.172	81×134	3.435626	9.55
91×151	3.435484256	0.234	91×151	3.435618	10.73
101×168	3.435510136	0.344	101×168	3.435597	13.01
111×184	3.435476480	0.437	111×184	3.435615	15.56
121×201	3.435515232	0.530	121×201	3.435596	18.65

(b)

Proposed method (quasi-TM mode)			BeamPROP		
Mesh size (M+1)×(N+1)	n_{eff}	CPU (sec.)	Mesh size (M+1)×(N+1)	n_{eff}	CPU (sec.)
11×18	3.436411608	<<0.01	11×18	3.435651	1.26
21×34	3.435670796	0.011	21×34	3.435422	1.90
31×51	3.435643808	0.0309	31×51	3.435470	2.98
41×68	3.435622804	0.047	41×68	3.435313	3.89
51×84	3.435337612	0.109	51×84	3.435360	5.55
61×101	3.435375552	0.218	61×101	3.435345	8.23
71×118	3.435398308	0.312	71×118	3.435386	10.60
81×134	3.435250344	0.452	81×134	3.435383	14.25
91×151	3.435284436	0.672	91×151	3.435384	17.30
101×168	3.435310460	0.844	101×168	3.435372	20.46
111×184	3.435270008	1.344	111×184	3.435383	24.33
121×201	3.435325920	1.452	121×201	3.435371	29.46

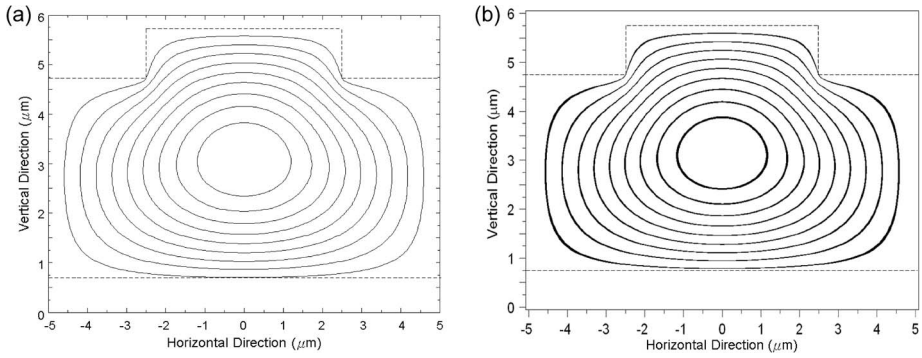

Fig. 5. Scalar mode contour with field levels at 10% to 90% of the maximum at an interval of 10% obtained by (a) the proposed method (121 × 201 points) and (b) BeamPROP.

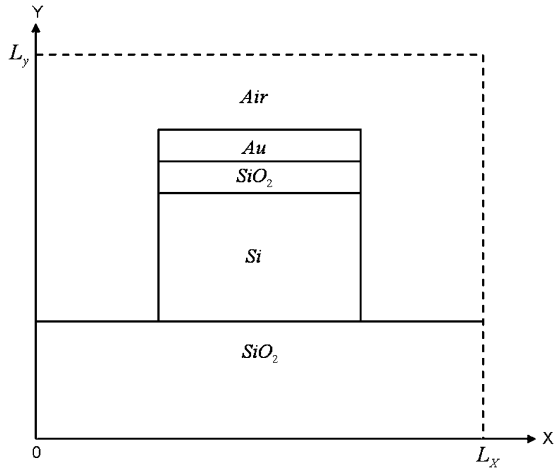

Fig. 6. A conductor-gap-silicon plasmonic waveguide for numerical demonstration in this study.

shown in Fig. 6, where the waveguide cross section consists of a SiO_2 slab and a metal-dielectric rib. In particular, the metal-dielectric rib consists of a thin SiO_2 layer sandwiched by a Si layer and a thin Au layer.

In the numerical simulation, we designate the thickness of the SiO_2 layer with the index $n_{SiO_2} = 1.44$, the Si layer with the index $n_{Si} = 3.48$, and the Au layer with the dielectric constant $\varepsilon_{Au} = -132 - 12.65 \cdot \tilde{j}$ $(\tilde{j} = \sqrt{-1})$ to 70 nm, 330 nm, and 50 nm, respectively, while the width of the metal-dielectric rib is fixed to 200 nm. These parameters are intentionally designated for the purpose that we can investigate whether the calculated field contour possesses the same features as those have been referred in [26]. Fig. 7(a) gives the calculated the magnitude of the field contour of the hybrid guided mode at 1550 nm in the CGS plasmonic waveguide. Fig. 7(b) shows the magnitude of the field contour along the *y*-direction at the center of the waveguide, i.e., at $x = 0$ (μm) in Fig. 7(a). It shows that a gap mode appears inside the SiO_2 gap layer. The corresponding profile of the gap mode is in good agreement with the one shown in [26]. Furthermore, Fig. 7(c) shows the magnitude of the field contour along the *x*-direction at the interface between the metal layer and SiO_2 layer, i.e., at $y = 0.4$ (μm) in Fig. 7(a). The resulting field contour is also in good agreement with the one shown in [26]. Both of the features mentioned in Fig. 7(b) and (c) reveal that the field contour calculated by the modified quasi-TM mode algorithm has the same features as those of the hybrid guided mode in the CGS plasmonic waveguide [26].

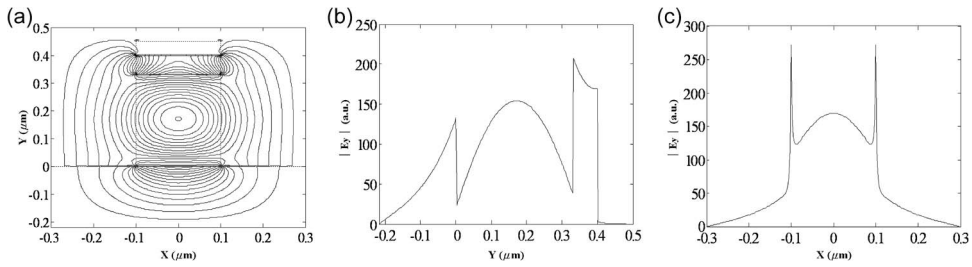

Fig. 7. (a) Quasi-TM hybrid guided mode contours with field levels at 3.3% to 100% of the maximum at an interval of 3.3% obtained by the modified quasi-TM mode algorithm (284 × 243 points). The thickness of the SiO_2 gap layer is designated to 70 nm. (b) The magnitude of the field contour along the y-direction at the center of the waveguide. (c) The magnitude of the field contour along the x-direction at the interface between the metal layer and the gap layer.

TABLE 4

Quasi-TM modal indices calculated by the modified method for the conductor-gap-silicon, plasmonic waveguide shown in Fig. 6

Mesh size (M+1)×(N+1)	Grid size △: (μm)	$(n_{eff})_{real}$	$(n_{eff})_{imag}$	CPU (sec.)
50×43	0.015	2.05675936	-0.00253855	0.078
74×63	0.010	2.00333608	-0.00197084	0.270
144×123	0.005	1.98440291	-0.00142838	2.486
284×243	0.0025	1.97598838	-0.00120489	26.25
354×303	0.002	1.97438817	-0.00116109	58.25

In addition to the calculation of the field contours, we may apply the modified quasi-TM mode method to investigate the modal indices of the CGS plasmonic waveguide. Table 4 shows that given a fixed computational window size $\Omega = L_x \times L_y = 0.6 \times 0.7\ (\mu m)^2$, the modified quasi-TM method with the grid size $\Delta = 0.0025\ \mu$m (284 × 243 mesh points) gives a convergent mode index. The corresponding mode index values calculated by the modified method converge to $n_{eff} = 1.97598838 - 0.00120489 \cdot \tilde{j}$ within 26.25 sec.

We apply the commercial tool COMSOL to investigate the modal properties of the conductor-gap-silicon plasmonic waveguide structure shown in Fig. 6. The size of the computational window $\Omega = L_x \times L_y$ is fixed to $10 \times 10\ (\mu m)^2$ and the mesh is more finely spaced (we designate the grid size to 0.1 nm) in the local regions near the metal-dielectric interface than the evanescent regions (we designate the grid size to 100 nm). We apply 34853 elements in the computational window to calculate the modal field and the modal indices. As a result, the calculated modal index reaches to $n_{eff} = 1.978129 - 0.002028 \cdot \tilde{j}$. Compared this result to Table 4, we can see the relative error for both real and imaginary parts of the effective index can reach to 10^{-4}. Meanwhile, the field contour calculated by the COMSOL is in good agreement with Fig. 7 and the one shown in [26].

6. Conclusion

An efficient method to calculate the modal indices and the modal fields for both scalar and quasi-TM waveguide modes is proposed in this paper. The modal indices and the corresponding modal fields of either a weakly guiding, GaAs-on-AlGaAs rib-type waveguide or a strongly guiding, silicon-on-insulator rib-type waveguide calculated by the proposed methods have been shown to be in a good agreement with the results referred in [24], [25] and/or those calculated

by BeamPROP. The quasi-TM method is applied to investigate the modal properties of the conductor-gap-silicon plasmonic waveguide. The feature of the hybrid guided mode profile presented in [26] is also observable from the field contour calculated by the quasi-TM method.

The semivectorial analysis of the today's complex waveguide structure, e.g., Si-based hybrid plasmonic waveguide [26] or SOI nano-wire with a metal cap [27] has been widely used in the past few years. The previous frameworks [26], [27] have shown that the field distribution of the major component of the quasi-TM fundamental mode in these plasmonic waveguide structures numerically calculated by employing the well-known FEM mode solver can accurately present the characteristic of the nano-scale field enhancement in the thin-SiO_2 layer. Thus the semivectorial mode solver still can be regarded as the useful tool to theoretically study the nano-scale optical waveguide. Meanwhile, the numerical results presented in Fig. 7 demonstrate that the proposed quasi-TM method is both accurate and efficient in the modal calculation of the hybrid plasmonic waveguide [26]. Such accurate results have proved the presented method's usefulness to the today's nano-scale waveguide structures.

The content in Sections 2 or 3 describes a very general process to solve the optical waveguide problems. The stationary solutions of the functional (2) and (11) are the modal field solutions of the corresponding wave equations (1) and (10) because their Euler–Lagrange equations are identical to the wave equations (1) and (10) [23]. Once such variation functional expression for any kind of waveguide problem (scalar/semivectorial/full-vectorial) is successfully established, we can use the dynamic programming technique to derive the accurate stationary solution in an efficient manner [17], [18]. Today, the variation functional expression with respect to the full-vectorial wave equation has been fully established, it is very straightforward to solve the stationary solution of the full-vectorial functional problem in terms of the dynamic programming technique described in this paper.

Acknowledgement

The authors would like to thank Prof. C. S. Hsiao of the Department of Photonics and Communication Engineering, Asia University, Taiwan, for his constructive and valuable suggestions.

References

[1] R. K. Lagu and R. V. Ramaswamy, "A variational finite-difference method for analyzing channel waveguides with arbitrary index profiles," *IEEE J. Quantum Electron.*, vol. QE-22, no. 6, pp. 968–976, Jun. 1986.
[2] B. M. A. Rahman and J. B. Davies, "Finite-element analysis of optical and microwave waveguide problems," *IEEE Trans. Microw. Theory Tech.*, vol. MTT-32, no. 1, pp. 20–28, Jan. 1984.
[3] T. Angkaew, M. Matsuhara, and N. Kumagai, "Finite-element analysis of waveguide modes: A novel approach that eliminates spurious modes," *IEEE Trans. Microw. Theory Tech.*, vol. MTT-35, no. 2, pp. 117–123, Feb. 1987.
[4] S. Akiba and H. A. Haus, "Variational analysis of optical waveguides with rectangular cross section," *Appl. Opt.*, vol. 21, no. 5, pp. 804–807, Mar. 1982.
[5] I. V. Lindell and M. I. Oksanen, "Asymptotic analysis of weakly guiding anisotropic optical fibers," *J. Opt. Soc. Amer. A, Opt. Image Sci.*, vol. 1, no. 1, pp. 87–95, Jan. 1984.
[6] A. Hardy, M. Itzkowitz, and G. Griffel, "Use of a variational moment method in calculating propagation constants for waveguides with an arbitrary index profile," *Appl. Opt.*, vol. 28, no. 10, pp. 1910–1913, May 1989.
[7] W. P. Huang, "Polarization correction of dispersion characteristics of optical waveguides," *Opt. Lett.*, vol. 15, no. 19, pp. 1052–1054, Oct. 1990.
[8] W. Huang and H. A. Haus, "A simple variational approach to optical rib waveguides," *J. Lightw. Technol.*, vol. 9, no. 1, pp. 56–61, Jan. 1991.
[9] Y. Boim and A. Hardy, "Application of the variational-moment method to symmetric and nonsymmetric waveguides," *Appl. Opt.*, vol. 33, no. 24, pp. 5642–5649, Aug. 1994.
[10] G. W. Wen, "Steepest-descent approximation theory for guided modes of weakly guiding optical waveguides and fibers," *J. Opt. Soc. Amer. A, Opt. Image Sci.*, vol. 8, no. 2, pp. 295–302, Feb. 1991.
[11] A. Sharma, P. K. Mishra, and A. K. Ghatak, "Single-mode optical waveguides and directional couplers with rectangular cross section: A simple and accurate method of analysis," *J. Lightw. Technol.*, vol. 6, no. 6, pp. 1119–1125, Jun. 1988.
[12] A. Sharma, "On approximate theories of single-mode rectangular waveguides," *Opt. Quantum Electron.*, vol. 21, no. 6, pp. 517–520, Nov. 1989.
[13] A. Sharma and P. Bindal, "An accurate variational analysis of single-mode diffused channel waveguides," *Opt. Quantum Electron.*, vol. 24, no. 12, pp. 1359–1371, Dec. 1992.

[14] K. Gehlot and A. Sharma, "Semi-vector iterative method for modes of high-index-contrast nanoscale waveguides," *Opt. Exp.*, vol. 21, no. 8, pp. 9807–9812, Apr. 2013.
[15] A. K. Taneja and E. K. Sharma, "Closed-form variational effective-index analysis for diffused optical channel waveguides," *J. Opt. Soc. Amer. A, Opt. Image Sci.*, vol. 16, no. 11, pp. 2781–2785, Nov. 1999.
[16] K. S. Chiang, "Analysis of the effective-index method for the vector modes of rectangular-core dielectric waveguides," *IEEE Trans. Microw. Theory Tech.*, vol. 44, no. 5, pp. 692–700, May 1996.
[17] R. Bellman, *Dynamic Programming*. Princeton, NJ, USA: Princeton Univ. Press, 1957.
[18] E. Angel and R. Bellman, *Dynamic Programming and Partial Differential Equations*. New York, NY, USA: Academic, 1972.
[19] N. Mabaya, P. E. Lagasse, and P. Vandenbulcke, "Finite element analysis of optical waveguides, "*IEEE Trans. Microw. Theory Tech.*, vol. MTT-29, no. 6, pp. 600–605, Jun. 1981.
[20] S. M. Saad, "Review of numerical methods for the analysis of arbitrarily-shaped microwave and optical dielectric waveguides," *IEEE Trans. Microw. Theory Tech.*, vol. MTT-33, no. 10, pp. 894–899, Oct. 1985.
[21] B. M. A. Rahman, F. A. Fernandez, and J. B. Davies, "Review of finite element methods for microwave and optical waveguides," *Proc. IEEE*, vol. 79, no. 10, pp. 1442–1448, Oct. 1991.
[22] K. Kawano and T. Kitoh, *Introduction to Optical Waveguide Analysis: Solving Maxwell's Equations and the Schrodinger Equation*, 1st ed. New York, NY, USA: Wiley-Interscience, 2001.
[23] R. Courant and F. John, *Introduction to Calculus and Analysis*, vol. 2. New York, NY, USA: Wiley, 1974.
[24] G. M. Berry, S. V. Burke, C. J. Smartt, T. M. Benson, and P. C. Kendall, "Exact and variational Fourier transform methods for analysis of multilayered planar waveguides," *IEE J. Proc. Optoelectron.*, vol. 142, no. 1, pp. 66–75, Feb. 1995.
[25] R. A. Soref, J. Schmidtchen, and K. Petermann, "Large single-mode rib waveguides in GeSi-Si and Si-on-SiO2," *IEEE J. Quantum. Electron.*, vol. 27, no. 8, pp. 1971–1974, Aug. 1991.
[26] M. Wu, Z. Han, and V. Van, "Conductor-gap-silicon plasmonic waveguides and passive components at subwavelength scale," *Opt. Exp.*, vol. 18, no. 11, pp. 11728–11736, May 2010.
[27] D. Dai and S. He, "A silicon-based hybrid plasmonic waveguide with a metal cap for a nano-scale light confinement," *Opt. Exp.*, vol. 17, no. 19, pp. 16 646–16 653, Sep. 2009.